Brain Struct Funct
DOI 10.1007/s00429-015-1108-6

ORIGINAL ARTICLE

Three-dimensional and stereological characterization of the human *substantia nigra* during aging

Ana Tereza Di Lorenzo Alho[1,2,3] · Claudia Kimie Suemoto[1,4] · Lívia Polichiso[1] · Edilaine Tampellini[1] · Kátia Cristina de Oliveira[1,2] · Mariana Molina[1] · Glaucia Aparecida Bento Santos[1,3] · Camila Nascimento[1] · Renata Elaine Paraizo Leite[1,4] · Renata Eloah de Lucena Ferreti-Rebustini[1,4] · Alexandre Valotta da Silva[1,3] · Ricardo Nitrini[1,5] · Carlos Augusto Pasqualucci[1,7] · Wilson Jacob-Filho[1,4] · Helmut Heinsen[2,7] · Lea Tenenholz Grinberg[1,6,7]

Received: 18 June 2015 / Accepted: 5 September 2015

Abstract The human brain undergoes non-uniform changes during aging. The *substantia nigra* (*SN*), the source of major dopaminergic pathways in the brain, is particularly vulnerable to changes in the progression of several age-related neurodegenerative diseases. To establish normative data for high-resolution imaging, and to further clinical and anatomical studies we analyzed SNs from 15 subjects aged 50–91 cognitively normal human subjects without signs of parkinsonism. Complete brains or brainstems with *substantia nigra* were formalin-fixed, celloidin-mounted, serially cut and Nissl-stained. The shapes of all SNs investigated were reconstructed using fast, high-resolution computer-assisted 3D reconstruction software. We found a negative correlation between age and *SN* volume ($p = 0.04$, rho $= -0.53$), with great variability in neuronal numbers and density across participants. The 3D reconstructions revealed *SN* inter- and intra-individual variability. Furthermore, we observed that human *SN* is a neuronal reticulum, rather than a group of isolated neuronal islands. Caution is required when using *SN* volume as a surrogate for *SN* status in individual subjects. The use of multimodal sequences including those for fiber tracts may enhance the value of imaging as a diagnostic tool to assess *SN* in vivo. Further studies with a larger sample size are needed for understanding the structure–function interaction of human SN.

Keywords Aging brain · *Substantia nigra* · Stereology · 3D reconstruction · Celloidin mounting

H. Heinsen has contributed equally.

✉ Lea Tenenholz Grinberg
lea.grinberg@ucsf.edu

1 Grupo de Estudos em Envelhecimento Cerebral e LIM 22, Department of Pathology, Faculdade de Medicina da Universidade de Sao Paulo, Av. Dr. Arnaldo, 455 sala 1353, São Paulo CEP 01246-903, Brazil

2 Labor für Morphologische Hirnforschung der Klinik und Poliklinik für Psychiatrie und Psychotherapie, Institut Rechtsmedizin, Universitätsklinikum Würzburg, Würzburg, Germany

3 Instituto do Cérebro, Hospital Israelita Albert Einstein, São Paulo, Brazil

4 Discipline of Geriatrics, Faculdade de Medicina da Universidade de São Paulo, São Paulo, Brazil

5 Department of Neurology, Faculdade de Medicina da Universidade de São Paulo, São Paulo, Brazil

6 Memory and Aging Center, Department of Neurology, University of California, San Francisco, USA

7 Department of Pathology, Faculdade de Medicina da Universidade de Sao Paulo, São Paulo, Brazil

Introduction

The number of individuals over 60 years old is expected to more than triple worldwide by 2100 (Ferri et al. 2005; UN 2013). The healthy human brain changes qualitatively and quantitatively during the lifespan (Sohmiya et al. 2001; Esiri 2007). After the fifth decade of life, the brain loses approximately 2–3 % of its weight and volume per decade (Esiri 2007). This loss is non-uniform because some areas are more vulnerable to aging than others (Pakkenberg et al. 1991; Esiri 2007; Di Giovanni et al. 2009; Cabello et al. 2002). The mesencephalic *substantia nigra* (*SN*), the principal source of dopaminergic projections to the basal ganglia, is particularly vulnerable to aging processes (Doraiswamy et al. 1992; Pujol et al. 1992). Furthermore, the *SN* is affected early in Parkinson disease (PD) and it can

Published online: 19 September 2015

also be involved in frontotemporal lobar degeneration and Alzheimer's disease (Braak et al. 2003a, b; Lyness et al. 2003; Grinberg et al. 2009, 2011; Kouri et al. 2011; Dickson 2012; raak and Braak 1991).

Imaging techniques are transforming neuroscience by facilitating the visualization of brain structures in vivo. *SN* imaging is a potential tool for diagnosing and monitoring the progression of PD, and its utility may extend to the investigation of other neurodegenerative diseases (Ogisu et al. 2013). However, a lack of validated normative data derived from morphological studies, especially in older individuals, hampers interpretation of *SN* imaging data (Pakkenberg et al. 1991; Ma et al. 1999; Cabello et al. 2002; Alladi et al. 2009). In order to characterize morphologically the *SN* in older individuals, we used design-based stereology, in which methods are independent of neuronal size, shape, spatial orientation, therefore, deemed unbiased (Schmitz et al. 1999a; Schmitz and Hof 2000) and 3D reconstructions to examine inter- and intra-individual differences in *SN* volume, neuronal population, neuronal density, and asymmetry. Our aim is to provide unbiased estimations to inform the establishment of normative values for application to future imaging, clinical, and anatomical studies of the *SN*.

Participants and methods

This study was approved by the ethical committees _ENREF_23 of the University of Sao Paulo and the University of Würzburg. Written informed consent for brain donation and provision of clinical information was obtained from the next-of-kin.

Participants

We studied the intact brainstems of 15 individuals: 14 were obtained from the Brain Bank of the Brazilian Aging Brain Study Group (BB-BABSG), University of Sao Paulo (Grinberg et al. 2007) and one was obtained from the University of Würzburg. These individuals were ≥50 years old at death and showed no cognitive decline (clinical dementia rating, CDR = 0, and informant questionnaire on cognitive decline in the elderly, IQCODE = 3.00) or parkinsonian symptoms (Morris 1993; Jorm 1994; Tanner et al. 1990). They had no signs of macroscopic brain infarcts, hemorrhage, or trauma. Cases were excluded from the study if Lewy bodies were identified anywhere in the brainstem. In addition, cases were selected to represent evenly both genders and a range of ages (see Table 1). For the Brazilian cases, a validated semi-structured interview was conducted with a knowledgeable informant who had at least weekly contact with the subject over the 6 months anteceding their death. _ENREF_24_ENREF_25 Clinical information for the German case was obtained from medical records.

In addition of the 15 cases, we used serial unstained sections through the brainstem of a 72-year-old female, and serial gallocyanin-stained sections from an entire brain of a 71-year-old female to facilitate interpretation of the results and for illustration purposes. These cases were not included in the subsequent analyzes.

Brain processing

Upon procurement, the total brain volume was obtained using a volume displacement method (Archimedes' principle) (Mouton 2011), as previously described in the BB-BABSG protocol (Grinberg et al. 2007). Brains were fixed in 4 % formalin. After that, the brainstem and cerebellum were severed with a cut ventral to the superior *colliculi,* to produce a brainstem block that included the whole *SN*. The brainstem blocks were embedded in celloidin and serially sectioned on a sliding microtome (Polycut, Cambridge Instruments, UK) with a section thickness of 350 µm (Heinsen et al. 2000; Theofilas et al. 2014). To evaluate the effect of the cutting axis to 3D reconstructions, the brainstems were cut in different orientations (see Table 1 for details). Slices were stained with gallocyanin (Nissl staining) and mounted, as previously described (Heinsen and Heinsen 1991).

Computer-assisted 3D reconstruction of the *SN*

Images were obtained during the cutting process by photographing the blockface using a camera (Canon EOS 5D Mark II 21.1 Megapixel®, Tokyo, Japan) mounted on the microtome knife holder The *SN* borders were defined on each section using a stereomicroscope, and drawn directly onto the corresponding digital image. The *SNs* were then reconstructed in 3D using the software Amira 5.3® (Mercury Systems), that uses state-of-the-art algorithms for segmentation and 3D reconstruction rendering high-resolution surfaces composed of several millions of triangles based on individual outlines in a smooth manner without delay (Heinsen et al. 2004; Theofilas et al. 2014).

Stereological measurements

We estimated neuronal numbers using the fractionator method with an optical disector probe. Results derived by this method are invulnerable to tissue shrinkage or changes in slide orientation. Each side of the *SN* was counted separately. We took several steps to abide by the principles

Table 1 Demographics, cause of death, measures of neurons in each study subject ($n = 15$)

Case	Age	Gender	SN side	Cutting plane	Number of neurons per side	Number of neurons (% asymmetry)	Total number of neurons	Volume per side (mm^3)	Volume (% asymmetry)	Total volume (mm^3)	Neuron density per side (neuron/mm^3)	Density (% asymmetry)	Mean neuron density (neuron/mm^3)
1	50	F	R	Frontal	576,431	+25	1,314,478	88	+14	190	7234	+0	7235
			L		738,047			102			7235		
2	50	M	R	Sagittal	686,869	−31	1,190,573	116	−22	209	5907	−8	5666
			L		503,704			92			5426		
3	52	M	R	Sagittal	839,058	−14	1,569,698	107	−14	200	7834	+0	7841
			L		730,64			93			7847		
4	55	F	R	Frontal	588,047	+3	1,193,771	96	+2	194	6087	+1	6123
			L		605,724			98			6158		
5	57	F	R	Sagittal	616,701	+27	1,427,880	90	+20	201	6818	+7	7064
			L		811,179			110			7310		
6	60	F	R	Sagittal	732,659	−18	1,341,415	127	−22	230	5741	+3	5843
			L		608,755			102			5944		
7	65	M	R	Frontal	707,071	−20	1,286,869	66	+2	133	10,688	−21	9658
			L		579,798			67			8627		
8	66	M	R	Sagittal	763,637	+13	1,630,978	136	−4	267	5594	+17	6110
			L		867,341			130			6625		
9	71	M	R	Sagittal	622,222	+41	1,569,697	89	+28	195	6971	+24	7938
			L		947,475			106			8904		
10	74	F	R	Frontal	367,677	−17	678,788	81	−1	162	4489	−15	4168
			L		311,111			80			3848		
11	77	M	R	Frontal	315,960	+53	860,876	69	+0	138	4577	+53	6236
			L		544,916			69			7895		
12	78	F	R	Horizontal	763,636	−16	1,414,141	94	−17	174	8080	+1	8116
			L		650,505			79			8151		
13	82	F	R	Sagittal	494,545	+34	1,195,151	70	+17	154	6993	+18	7684
			L		700,606			83			8376		
14	83	M	R	Frontal	694,950	−15	1,292,930	100	−11	190	6921	−4	6797
			L		597,980			89			6673		
15	91	F	R	Frontal	405,387	+33	971,044	91	+26	188	4454	+26	5134
			L		565,657			97			5813		

Gender: M, male; F, female; SN side: R, right; L, left; asymmetry: +, left side; −, right side

of design-based stereology. We manually overlaid a transparent grid ($d = 1$ mm) onto each histological slide (West 1993). After that, we photographed the grid's crossing points hitting the *SN* with a Fuji FinePix S2 Pro® camera (Tokyo, Japan) mounted with a SIGMA® macro lens (1:2.8, 50 mm). Each crossing point became a disector (counting frame-area: 0.02 mm^2) analyzed at a magnification of 400× (objective 40:1.0, 10 wide field eyepieces). The disector height was established at 29.7 µm, with the superior point set at the appearance of the first neuron in focus, plus a 15-µm guard zone. Pictures were taken at 11 different points along the z-axis at 2.7-µm intervals. The images were uploaded to ImageJ (National Institutes of Health, USA), a software that provides various stereological tools. We used the "cell counter" plugin, to transform the image stack of each counting frame in a virtual optical disector containing a z-axis scale. Each virtual disector was overlaid with a 100-μm^2 grid, and two forbidden lines were established. All neurons with neuromelanin and lipofuscin granules in the *SN pars compacta* (*SNpc*) and *SN pars diffusa* (*SNdiff*)_ENREF_32 were counted manually. Each nucleolus coming anew to focus within the disector was counted (van Domburg and ten Donkelaar 1991).

The total number of neurons was calculated using Eq. (1), where $\sum Q$ was the sum of counted nucleoli, t was the mean section thickness, h was the height of the disector, asf was the area sampling fraction, and ssf was the section sampling fraction (1, since every slice was evaluated) (West 1993; Heinsen et al. 1994, 2000). The coefficient of error (CE) was calculated using Eq. (2) (West et al. 1996).

$$\text{Neuronal number} = \sum Q \times \frac{t}{h} \times \frac{1}{\text{asf}} \times \frac{1}{\text{ssf}} \tag{1}$$

$$\text{CE} = \sqrt{\text{CE}^2\left(\sum Q^{-}\right) + \text{CE}^2(t)} \tag{2}$$

The *SN* volume was estimated using the Cavalieri principle (3), multiplying the total sum of crossing points hitting *SN* ($\sum Q_i$) by the grid area [$a(p)$] and t (mean section thickness). The CE was calculated using Eq. (4) (Gundersen and Jensen 1987).

$$\text{Volume} = \sum Q_i \times a(p) \times t \tag{3}$$

$$\text{CE} = \left(\sum_{i=1}^{n} A_i\right)^{-1} \times \left[\frac{1}{12}\left(3\sum_{i=1}^{n} A_i^2 + \sum_{i=1}^{n-2} A_i A_{i+2} - 4\sum_{i=1}^{n-1} A_i A_{i+1}\right)\right] \tag{4}$$

The neuronal density was then calculated by dividing the total number of neurons by the *SN* total volume (Heinsen et al. 2000).

An asymmetry coefficient (δ) was calculated for each case (Eidelberg and Galaburda 1982). For each variable, we used Eq. (5), where Xl represented the left-side value and Xr represented the right-side value_ENREF_36.

$$\delta = \frac{\text{Xl} - \text{Xr}}{0.5\ (\text{Xl} + \text{Xr})} \tag{5}$$

Statistical analysis

Means, standard deviations, and minimum and maximum values were described for continuous variables while absolute and relative frequencies were used for categorical variables. We used the Spearman's rank coefficient to examine the correlation of age with the number of neurons, volume, and cell density. We further stratified these correlations by gender and brain side. In addition, we investigated the correlation between the *SN* total number of cells and volume using Spearman's rank test. Linear regression models were used to investigate the association between total brain volume and *SN* volume, adjusted for gender and age. The level of significance was set at 0.05 level in 2-sided tests. Statistical analyzes were performed with Stata 12.0 (StataCorp, College Station, TX, 2011).

Results

Morphological characteristics of the SN and 3D reconstructions

Our Nissl-stained thick sections showed clear-cut *SN* borders that facilitated delineation between the *SNpc*, components of the ventral tegmental area, and the *SN pars reticulata* (*SNret*). We confirmed previous reports that the *SN* extended from the caudal limits of the mammillary bodies to the rostral margin of the pons. The *SN* is covered ventrally by fibers of the cerebral peduncles, and dorsally by the crossing fibers of the superior cerebellar peduncle (Fig. 1a). A substantial portion of the efferent cerebellar fibers end in the red nucleus, forming the dorsorostral border of the anterior *SN* (Fig. 1a). We also could clearly visualize the two parts *of the SN* : the *SNpc*, with large (∼50 µm) neuromelanin-rich neurons, and the *SNret* composed of afferent fiber bundles, thick dendrites, and sparse neurons without neuromelanin granules (Lynd-Balta and Haber 1994). As stated by some authors (Braak and Braak 1986; Fearnley and Lees 1991; van Domburg and ten Donkelaar 1991; McRitchie et al. 1995), We also appreciated a third part, the *SNdiff*, with a low neuronal density and smaller neurons filled with lipofuscin and clusters of *SNpc*-like neurons; this was found between the dorsal and ventral tiers of the *SNpc* (Fig. 2).

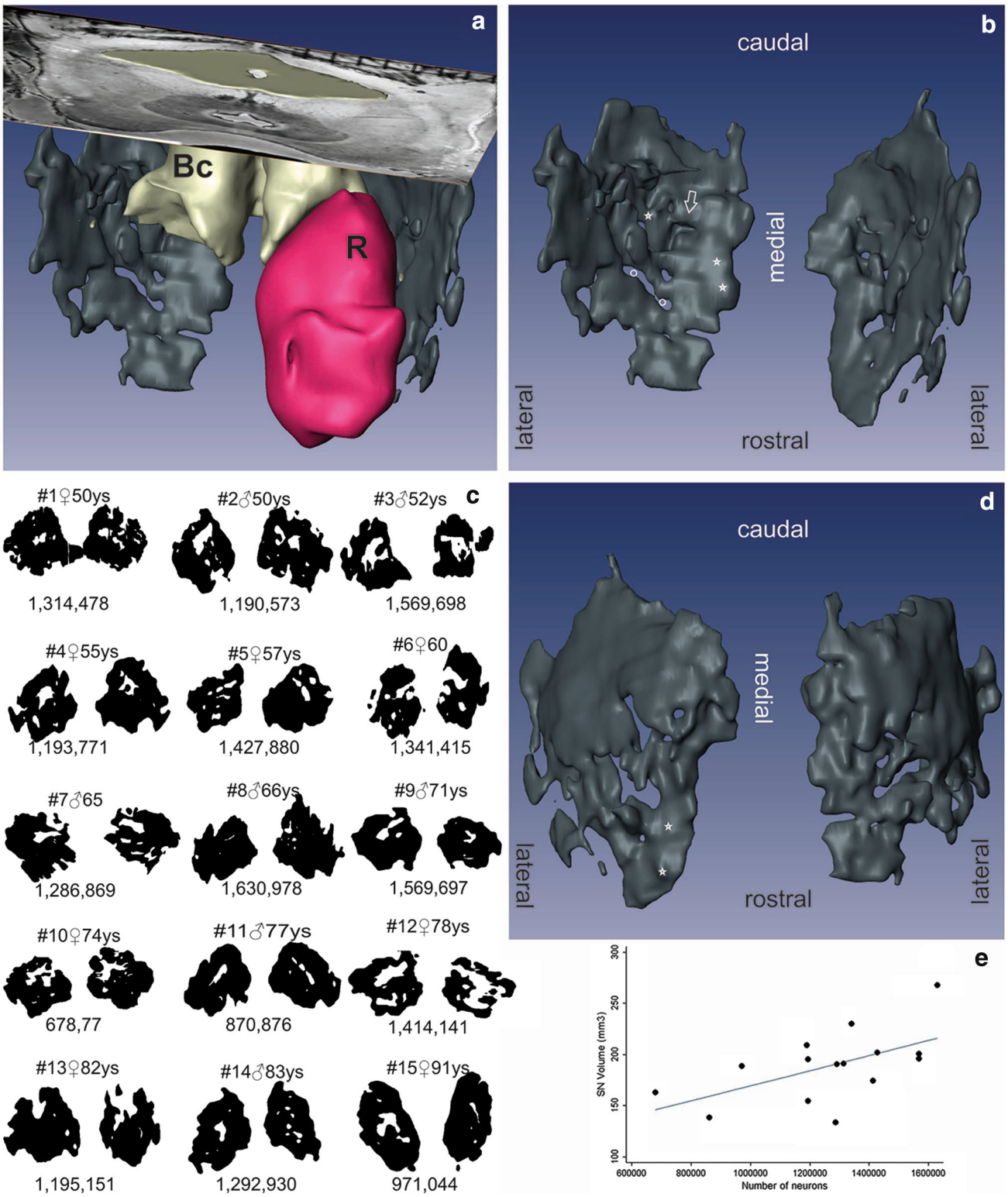

Fig. 1 3D **a** reconstruction of the *substantia nigra* (*SN*) (*black*) seen from dorsal. **b** Same as **a**, only *SN*. **c** Ventral aspect of the *SN*. **d** Reconstruction of the *SNs*. **e** Scatter plot of the *SN* volume and neuron numbers. Red nucleus (*R*); *brachium conjunctivum* (*BC*); *stars* cell clusters; *arrow* trough-like thinning, ending in a pouch; *white circles* central perforations

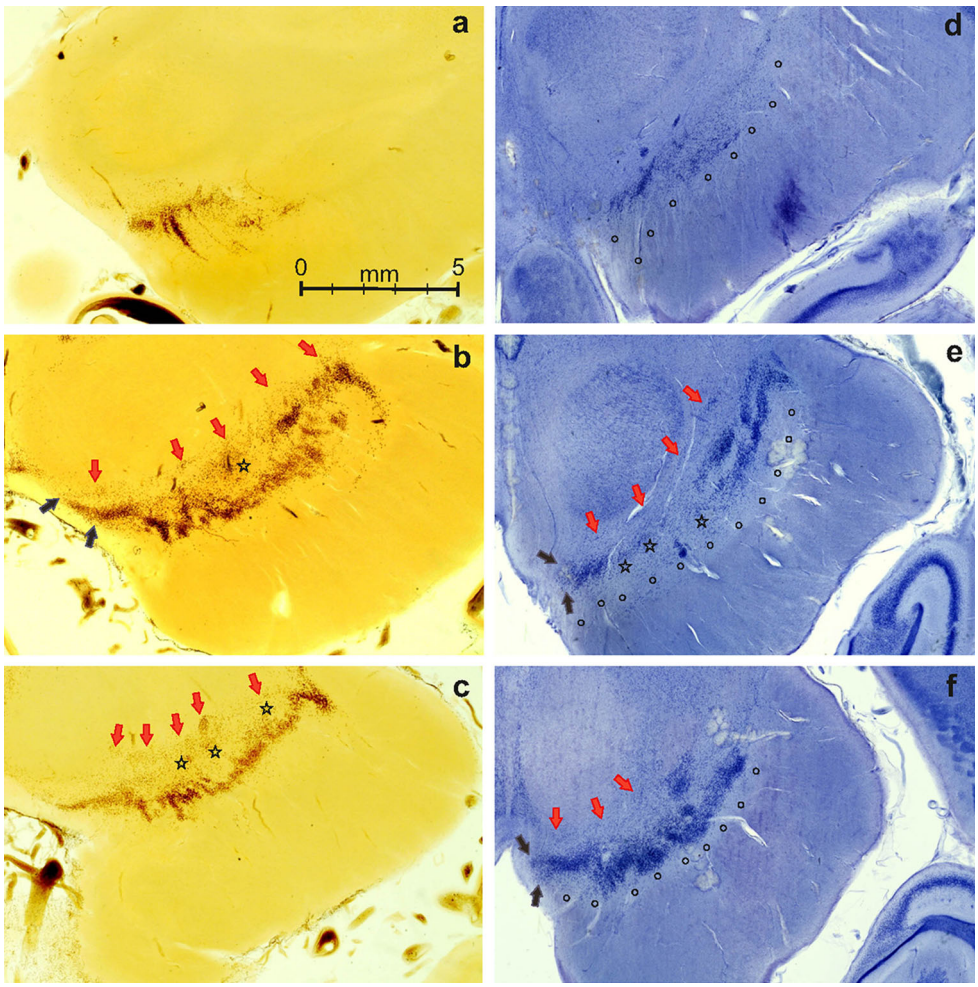

Fig. 2 *Substantia nigra* (*SN*) unstained sections from a 72-year-old female (**a**–**c**) and gallocyanin-stained sections from a 71-year-old female (**d**–**f**). *Arrows*: *red* parabrachial nucleus; *black* rostromedial and caudolateral border of paranigral nucleus. *Circles* indicate *SN pars reticulata* and *stars* indicate *SN pars diffusa*

We observed that the neurons of *SNpc* form one (at the rostral and caudal poles) or two beaded undulating dorsal and ventral bands, which may overlap, as seen before (Francois et al. 1985) (Fig. 2). The beaded appearance of the neuronal band is caused by parallel rostrocaudally extending cell clusters; these appeared to be connected by a thin single-cell layer of pigmented *SN* neurons, as seen in the Nissl-stained sections (Fig. 2, ventral tier). Furthermore, the undulating outlines of these bands were obviously caused by close attachment of *SN* neurons and clusters to descending fiber bundles within the *SNret* (Fig. 3). We noticed an absence of the dorsal band from central parts of the *SN*, which is characterized by large cell clusters with ill-defined boundaries, consisting of neurons with a low neuromelanin load, and located ventral to the dorsal band (Fig. 2, stars). In addition, the ventral band is regularly perforated (Fig. 2c), displaying a sieve-like appearance. In the subsequent serial section, the medial and lateral end of the ventral band of the SN appeared disconnected for about 2 mm, as shown in Fig. 2e.

In single histological sections, the profiles of the *SN* neuronal clusters varied considerably depending on the plane of section. Nevertheless, reconstructions derived from *SN*s cut in horizontal, sagittal, or frontal planes yielded similar 3D objects, as shown in Fig. 1d.

The 3D reconstructions show clearly that the *SNpc* resemble a perforated plate or neuronal reticulum closely attached to longitudinal fiber systems, rather than groups of neuronal islands. In its central part, this flat sheet was perforated by holes of variable sizes containing longitudinal fiber system (Fig. 1b, white circles). Other smaller clefts were distributed over the *SN* in an irregular manner. In addition, pockets and trough-like impressions (Fig. 1b, white arrow) were flanked by thicker, partly notch-like, rostrocaudally oriented cellular strands (Fig. 1, stars). The anterodorsal and anteroventral aspects of the *SN* presented a highly irregular surface, in contrast to the smooth caudoventral surface (Fig. 1).

Finally, we observed a marked intra- and inter-individual differences in shape and asymmetry. In about half cases, the left *SN* is bigger or had more neurons that the

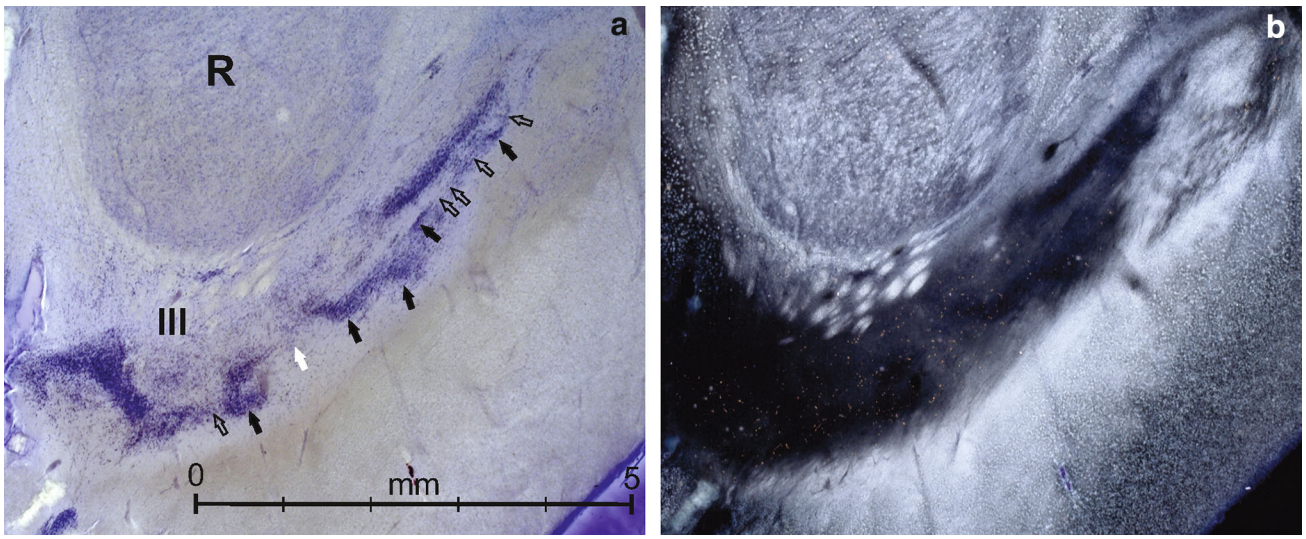

Fig. 3 **a** Gallocyanin-stained anterior part of the *substantia nigra (SN)* (dorsal tier) and **b** darkfield illumination of the same section from subject #1. *R* red nucleus; *III* rootlets of the oculomotor nerve. **a** *Black arrows* point to cell clusters, whereas *open arrows* point to single- or double-layered cell strands connecting the cell clusters. This is reminiscent of a net or mesh (latin *reticulum*) consisting of nodes (clusters) connected by neuronal bridges (strands) in a medio-lateral course. As a contrast, the *white arrow* in **a** points to a cleft between nodes not bridged by cell strands but representing instead a stream of cells seems to effuse in a dorso-ventral direction. By their size and staining properties these cells belong to the *pars diffusa*, and are oriented in parallel to a fiber tract, which is leaving or entering the *pars compacta reticulum* via a cleft or hole (cf. Fig. 1b, *white circles*)

right. Curiously in the remaining cases, the opposite was true (Table 1).

Stereological analysis

Table 1 gives the mean age, neuron numbers, *SN* volume and density of the 15 participants. The smallest neuronal number was found in a 74-year-old female (678,788 neurons), and the largest number was identified in a 66-year-old male (1,630,978 neurons). See Fig. 1d for details. The mean CE was 0.05 (range 0.01–0.1) and 0.01 (range 0.01–0.03) for neuronal population and volume estimation, respectively.

We found a moderate negative correlation between age and total *SN* volume (rho $= -0.53$, $p = 0.04$). In contrast, we did not find correlations between age and *SN* neuronal number (rho $= -0.22$, $p = 0.34$) or age and *SN* neuronal density (rho $= -0.03$, $p = 0.59$). In fact, *SN* neuronal number and *SN* volume were only moderately correlated ($r = 0.57$, $p = 0.03$).

Interestingly, we verified an association between *SN* volume and total brain volume. Each 1 mm^3 increased in brain volume, was associated with an average of 0.30 mm^3 increase in *SN* volume, adjusted for age and gender ($\beta = 0.30$, 95 % CI $= 0.10$–0.50, $p = 0.008$). Therefore, to verify if the observed age-dependent loss of *SN* volume was a mere effect of a possible age-dependent smaller brain volume, we analyzed if there was an association between total brain volume and age. This analysis was negative (Spearman's rho $= 0.01$ and $p = 0.97$), refuting the hypothesis.

The associations of age with *SN* volume, neuronal number, or neuronal density were not significant when the sample was stratified by gender or brain side (Table 2).

Discussion

Our results were consistent with those of previous studies, identifying a clear *SN* division into *pars compacta*, *reticulata*, and *diffusa*, and confirming the highly inter-individual variation in shape, neuron number, and volume of the *SN* (Braak and Braak 1986; German et al. 1983; McRitchie et al. 1995). In addition, the present study of 15 older adults with normal cognition and no parkinsonism from different age groups produced three major findings of relevance. First, older age was associated with smaller *SN* volume but *SN* neuronal number remained stable. Second, 3D reconstructions revealed a novel feature of the *SN*, showing the *SNpc*/*SNdiff* as a neuronal reticulum perforated by fibers. Third, intra-individual *SN* asymmetry is the norm but follows an unpredictive pattern.

The identified stable neuronal population and density numbers along aging, despite a significant age-dependent decrease in *SNpc*/*SNdiff* volume seems paradoxical. This apparently disproportionate volume decrease is likely correlated to factors independent of neuronal numbers, such as atrophy of neuronal processes (dendrites, axons), or a

Table 2 Correlation between SN neuronal number, volume, neuronal density and age ($n = 15$)

	Side	Female		Male		Female + male	
		Spearman's rho	p value	Spearman's rho	p value	Spearman's rho	p value
Number of neurons	R	−0.2857	0.49	−0.4286	0.34	−0.2788	0.31
	L	−0.3810	0.35	0.2500	0.59	−0.2073	0.46
	R + L	−0.2857	0.49	−0.0714	0.88	−0.2627	0.34
Volume	R	−0.1905	0.65	−0.3571	0.43	−0.2645	0.34
	L	−0.5952	0.12	−0.1429	0.76	−0.3610	0.191
	R + L	−0.5952	0.12	−0.4286	0.34	−0.5344	**0.04**
Neuronal density	R	−0.2857	0.49	−0.3214	0.48	−0.2288	0.41
	L	0	1.00	0.3214	0.48	−0.1501	0.59
	R + L	−0.0714	0.87	0.1429	0.76	−0.0340	0.90

Bold value is statistically significant

Side: *R* right, *L* left

decrease in neuronal size, resulting in smaller gaps between neurons (Ma et al. 1999). It is important to stress that the optical fractionator quantifies absolute numbers, rather than cell volume what could explain the dissociation between individual *SN* volume and neuronal population. The majority of other stereological studies on SN aging with number of control subjects varying between 7 and 19 subjects and age >50 years described results in line with ours (Pakkenberg et al. 1991; Halliday et al. 1996; Muthane et al. 1998; Chu et al. 2002; Alladi et al. 2009; Kubis et al. 2000). Only three groups found an age-related decrease in SN neuronal numbers.(Ma et al. 1999; Cabello et al. 2002). Nevertheless, direct comparisons should be avoided as the absolute numbers of neurons in the *SN* varied considerably in these studies. The range of results reported in previous articles (from around 180,000 TH + neurons (Kubis et al. 2000), passing through an average of 317,000 (Cabello et al. 2002) and 368,000 (single side) (Rudow et al. 2008) and finally around 810,000 pigmented neurons (Pakkenberg et al. 1991) may reflect the different selection criteria, sampling, staining, and counting protocols employed. Regarding selection criteria, other investigators selected controls based on review of medical charts rather than objective testing. Regarding sampling, in some instances, only one side (Rudow et al. 2008), or an incomplete *SN*, was available (Alladi et al. 2009; Perl et al. 2000). Our findings highligh the considerable intra-individual asymmetry of SN neuron number rendering extrapolation of results from single-side estimations to total SN neuron numbers obsolete. In addition, most unbiased stereological studies used 40-µm brainstem sections. Although such preparations meet criteria for unbiased estimations, the *SN* borders may not be as easy to define as in our 350-µm preparations (Fig. 2). Finally, most authors restricted neuronal counting to either neuromelanin-positive or tyrosine hydroxylase-positive neurons or did not state which neuronal types were counted (Rudow et al. 2008; Kubis et al. 2000). As our staining protocol bleaches neuromelanin, we were unable to distinguish neuromelanin-positive from neuromelanin free-neurons. Therefore, both neuronal types are included in our countings. Using a protocol that was similar to ours, Pakkenberg et al. (1991) estimated an average *SN* population (pigmented + non-pigmented neurons) of ~810,000 neurons, a figure that was closer to our data than those reported by other authors. Considering the highly irregular structure of the *SNpc/SNdiff* and the broad variability in neuronal density between *SN* regions, the still higher neuron numbers reported here are likely to result from the different counting protocol employed covering a greater field, including neuromelanin-negative neurons, and analyzing a higher number of nucleoli, which affect the estimation precision (Glaser and Wilson 1998; Schmitz 1998; Schmitz et al. 1999a, b). Pakkenberg et al. (1991) counted an average of 150 neuronal nuclei per case, whereas we counted at least 1200 per case.

A larger number of studies evaluated age-related changes in the *SN* using biased stereological methods. However, such results are unreliable and may under- or over-estimate neuronal number (Ma et al. 1995). It is also possible that factors specific to the Brazilian population or environment helped to preserve *SN* neurons during aging. A study by Alladi et al. (2009) used unbiased stereology to investigate *SN* changes across the lifespan in 32 Hindus. Consistent with the present study, they reported that age did not correlate significantly with neuronal number. The authors hypothesized that the ethnicity of their study population explained this conflict with previous reports of *SN* neuronal loss. A study including individuals of mixed ethnicities, from a range of geographical regions, would be necessary to verify these findings.

We found a positive correlation between total brain and *SN* volume. However, the lack of association between age

and total brain volume in this series refutes the hypothesis, that an age-dependent effect on *SN* volume could be dependent on a possible age-related smaller total brain volume.

Viewed two-dimensionally, the spatial arrangement of *SNpc*/*SNdiff* neuronal clusters resembled that reported by previous studies (Hassler 1937; McRitchie et al. 1995; German et al. 1983; Heinsen et al. 1994). However, our high-resolution 3D reconstructions unexpectedly revealed that in all cases, the *SNpc*/*SNdiff* neurons actually formed a perforated plate or coarse reticular network, rather than isolated islands of neurons as suggested previously (Hassler 1937; German et al. 1983). A previous study presented a *SN* 3D reconstruction of a 33-year-old man (German et al. 1983). This study pioneered in demonstrating *SN* shape, but it was limited by the computer power available at that time and because just one case was used. Therefore, the computer-assisted 3D reconstructions of the *SN* volume based on very thick serial histological sections, which are less prone to distortion, and the use of fast high-resolution computer techniques represent an important innovation of our study.

We hypothesize that the *SN* perforations represent the entrance or exit sites of fiber bundles connecting *SN* components and rostral di- and telencephalic structures. The dorsal tier receives afferents from the anterior and ventral striatum, whereas the ventrolateral tier is connected by dorsal striatal afferents (Haber et al. 2000). Studies in monkeys support our observation of the reticular nature of the *SNpc* (Lynd-Balta and Haber 1994). Lynd-Balta and Haber (1994) identified a close relationship between defined ventral striatal afferents and *SNpc* cell clusters in monkeys (see Fig. 3. of their article). Similar spatial relationships were shown in Fig. 12 of Hedreen and DeLong's article (1991). Both are comparable to our observations as seen in Fig. 2. Supporting this argument, Francois et al. (1985) described a large fiber bundle in the macaque *pars mixta,* which could represent a hilum for fibers leaving the *SN,* including nigrothalamic and nigrotegmental fibers. Hedreen and DeLong (1991) also highlighted the patchy nature and dense terminal fields of striatonigral projections in both the *SNret* and *SNpc*. Cellular clusters and intercluster constrictions (Fig. 1, stars), which are particularly concentrated at the transition between the dorsal and ventral tiers, could represent a negative impression of fiber tracts and terminals on the *SNpc* reticulum, indicating sites of interaction between parallel but segregated ventral and dorsal striatal afferents. This kind of interaction is of paramount importance for primate and human incentive-based learning, for the development of goal-directed behavior, and for habit formation (Haber and Behrens 2014). Curiously, this complex arrangement contrasts with the rather smooth and regular surface of the caudal ventrolateral tier, the target of afferents coming predominantly from the putamen (Hedreen and DeLong 1991; Lynd-Balta and Haber 1994). Neurons in the ventrolateral tier are particularly vulnerable to PD (Fearnley and Lees 1991; Halliday et al. 1996; Damier et al. 1999).

From the imaging investigation perspective, the crossing fibers confer the inter-individual differences in shape and volume of the *SN* and probably contribute for the relative disconnection between neuronal population size and *SN* volume. In fact, SN volume is not a good marker of SN neuronal population size (Fig. 1d). Together with immense individual variability with respect to the size, shape, and laterality of the *SN*, it suggests that simple voxel-based morphometric investigations of the *SN* using clinical imaging methods are unlikely to be informative. Previous investigation of basal ganglia volume and cell population in age- and sex-matched controls also did not identify a correlation between the neuronal number and volume (Kreczmanski et al. 2007). Further morphological studies focusing on fiber systems may provide information that could contribute to the development of a multimodal imaging package; this could enhance the practical utility of imaging in the investigation of the *SN*.

Parkinson disease shows an asymmetric clinical picture. We detected up to 53 % intra-individual side asymmetry for neuron number in the *SN*. We hypothesize that this difference in the number of neurons may contribute to the asymmetric manifestation of PD. As clinical severity is directly correlated to neuronal loss, we speculate the PD asymmetric presentation may be partially explained by one side of SN having less tissue reserve. Because we counted dopaminergic and non-dopaminergic neurons together, we cannot discard though that the observed asymmetry is more related to the latter. However, our observation suggests that a high degree of asymmetry also occurs in the dopaminergic neurons. The great majority of counted cells resembled big neurons with distributed Nissl substance, similar to the type I neurons described by Braak and Braak (1986). In fact, during extensive nucleolar counting, small neurons (classically neuromelanin-negative ones) represented less than 20 % of the total SNpc. This fact can be appreciated comparing the neuron density of Nissl-stained neurons in Figs. 2a–c with a similar density of neuromelanin-positive otherwise unstained neurons in Fig. 2d–f. Pakkenberg et al. (1991) reported that around 30 % of SN cells were non-pigmented.

Even though our sample size is similar to other investigations, the small absolute number of study subjects still represents a limitation of the present study. Therefore, we cannot exclude the possibility of a false negative result (type 2 error) regarding the lack of association between age and neuronal loss. Although a relatively large number of potential cases were available in the Brazilian brain bank,

our selection criteria were stringent, and only 1 in 3 of these were selected. In addition, the use of specialized software represents another limitation of this study. Automatic algorithms facilitated high-resolution 3D reconstruction of the *SN*, but the algorithm codes are not completely accessible to the end-user and may distort the final volumes. Distortions have been reported previously in the use of medical imaging software (Schmithorst et al. 2001). Also, post-mortem brain tissue suffers inherent distortion during processing. This could affect *SN* volume in an inter-individual and unpredictable way. We tried to minimize differences by using the same protocol for all the cases. Finally, as our series only included subjects older than 50 years, age-associated *SN* changes occurring before the 6th decade of life would be missed. Interestingly, Pakkenberg et al. (1991) initially reported no age-dependent neuron loss in *SNpc*/*SNdiff*, whereas a follow-up study that included younger subjects did report a statistically significant age-related neuron loss (Cabello et al. 2002).

In conclusion, our findings indicate that caution is required when using *SN* volume as a surrogate of *SN* neuronal numbers. The use of multimodal imaging including sequences for fiber tracts may enhance the value of imaging as a diagnostic tool to assess *SN* in vivo.

Acknowledgments We are grateful to the families that donated brains for this research. We would also like to thank all the members of the Brain Bank of the Brazilian Aging Brain Study Group. We are grateful to Prof. Dr. Edson Amaro Junior for scientific collaboration and Dr. Eduardo Alho for technical support in 3D reconstruction. We also thank Dr. Janet Johnston (http://www.output.ie) for language editing. Funding sources: Coordenacao de Aperfeicoamento de Pessoal de Nivel Superior (CAPES), Institute for Education and Research of Albert Einstein Hospital, São Paulo Research Foundation (FAPESP), Brazilian National Council for Scientific and Technological Development (CNPq), LIM-22 (HC-FMUSP) for research financial and technical support in Brazil, and the National Institutes of Health, USA (R01AG040311).

Compliance with ethical standards

Conflict of interest The authors declare that there are no conflicts of interest.

Ethical approval All procedures performed in studies involving human participants were in accordance with the ethical standards of the institutional and/or national research committee and with the 1964 Helsinki declaration and its later amendments or comparable ethical standards.

This study was approved by the ethical committees _ENREF_23 of the University of Sao Paulo and the University of Würzburg. Written informed consent for brain donation and provision of clinical information was obtained from the next-of-kin.

References

Alladi PA, Mahadevan A, Yasha TC, Raju TR, Shankar SK, Muthane U (2009) Absence of age-related changes in nigral dopaminergic neurons of Asian Indians: relevance to lower incidence of Parkinson's disease. Neuroscience 159:236–245

Braak H, Braak E (1986) Nuclear configuration and neuronal types of the nucleus niger in the brain of the human adult. Hum Neurobiol 5:71–82

Braak H, Braak E (1991) Neuropathological stageing of Alzheimer-related changes. Acta Neuropathol 82:239–259

Braak H, Del Tredici K, Rüb U, de Vos RA, Jansen Steur EN, Braak E (2003a) Staging of brain pathology related to sporadic Parkinson's disease. Neurobiol Aging 24:197–211

Braak H, Rüb U, Gai WP, Del Tredici K (2003b) Idiopathic Parkinson's disease: possible routes by which vulnerable neuronal types may be subject to neuroinvasion by an unknown pathogen. J Neural Transm 110:517–536

Cabello CR, Thune JJ, Pakkenberg H, Pakkenberg B (2002) Ageing of *substantia nigra* in humans: cell loss may be compensated by hypertrophy. Neuropathol Appl Neurobiol 28:283–291

Chu Y, Kompoliti K, Cochran EJ, Mufson EJ, Kordower JH (2002) Age-related decreases in Nurr1 immunoreactivity in the human *substantia nigra*. J Comp Neurol 450:203–214

Damier P, Hirsch EC, Agid Y, Graybiel AM (1999) The *substantia nigra* of the human brain. II. Patterns of loss of dopamine-containing neurons in Parkinson's disease. Brain 122(Pt 8):1437–1448

Di Giovanni G, Di Matteo V, Esposito E (2009) Birth, life and death of dopaminergic neurons in the *substantia nigra*. J Neural Transm Suppl 73:1

Dickson DW (2012) Parkinson's disease and parkinsonism: neuropathology. Cold Spring Harb Perspect Med 2(8). doi:10.1101/cshperspect.a009258.1

Doraiswamy PM et al (1992) Morphometric changes of the human midbrain with normal aging: MR and stereologic findings. AJNR Am J Neuroradiol 13:383–386

Eidelberg D, Galaburda AM (1982) Symmetry and asymmetry in the human posterior thalamus. I. Cytoarchitectonic analysis in normal persons. Arch Neurol 39:325–332

Esiri MM (2007) Ageing and the brain. J Pathol 211(2):181–187

Fearnley JM, Lees AJ (1991) Ageing and Parkinson's disease: *substantia nigra* regional selectivity. Brain 114(Pt 5):2283–2301

Ferri CP et al (2005) Global prevalence of dementia: a Delphi consensus study. Lancet 366:2112–2117

Francois C, Percheron G, Yelnik J, Heyner S (1985) A histological atlas of the macaque (Macaca mulatta) *substantia nigra* in ventricular coordinates. Brain Res Bull 14:349–367

German DC, Schlusselberg DS, Woodward DJ (1983) Three-dimensional computer reconstruction of midbrain dopaminergic neuronal populations: from mouse to man. J Neural Transm 57:243–254

Glaser EM, Wilson PD (1998) The coefficient of error of optical fractionator population size estimates: a computer simulation comparing three estimators. J Microsc 192(2):163–171

Grinberg LT et al (2007) Brain bank of the Brazilian aging brain study group—a milestone reached and more than 1600 collected brains. Cell Tissue Bank 8:151–162

Grinberg LT et al (2009) The dorsal raphe nucleus shows phospho-tau neurofibrillary changes before the transentorhinal region in Alzheimer's disease. A precocious onset? Neuropathol Appl Neurobiol 35:406–416

Grinberg LT, Rueb U, Heinsen H (2011) Brainstem: neglected locus in neurodegenerative diseases. Front Neurol 2:42

Gundersen HJ, Jensen EB (1987) The efficiency of systematic sampling in stereology and its prediction. J Microsc 147:229–263

Haber SN, Behrens TE (2014) The neural network underlying incentive-based learning: implications for interpreting circuit disruptions in psychiatric disorders. Neuron 83:1019–1039

Haber SN, Fudge JL, McFarland NR (2000) Striatonigrostriatal pathways in primates form an ascending spiral from the shell to the dorsolateral striatum. J Neurosci 20:2369–2382

Halliday GM, McRitchie DA, Cartwright H, Pamphlett R, Hely MA, Morris JG (1996) Midbrain neuropathology in idiopathic Parkinson's disease and diffuse Lewy body disease. J Clin Neurosci 3:52–60

Hassler R (1937) Zur Normalanatomie der *Substantia nigra*. Versuch einer architektonischen Gliederung. J Psychol Neurol 48:1–55

Hedreen JC, DeLong MR (1991) Organization of striatopallidal, striatonigral, and nigrostriatal projections in the macaque. J Comp Neurol 304:569–595

Heinsen H, Heinsen YL (1991) Serial thick, fronze, gallocyanin stained sections of human central nervous system. J Histotechnol 14:167–173

Heinsen H, Henn R, Eisenmenger W, Götz M, Bohl J, Bethke B, Lockemann U, Püschel K (1994) Quantitative investigations on the human entorhinal area: left–right asymmetry and age-related changes. Anat Embryol (Berl) 190(2):181–194

Heinsen H, Arzberger T, Schmitz C (2000) Celloidin mounting (embedding without infiltration)—a new, simple and reliable method for producing serial sections of high thickness through complete human brains and its application to stereological and immunohistochemical investigations. J Chem Neuroanat 20:49–59

Heinsen H, Arzberger T, Roggendorf W, Mitrovic T (2004) 3D reconstruction of celloidin-mounted serial sections. Acta Neuropathol 108(4):374

Jorm AF (1994) A short form of the Informant Questionnaire on Cognitive Decline in the Elderly (IQCODE): development and cross-validation. Psychol Med 24:145–153

Kouri N, Whitwell JL, Josephs KA, Rademakers R, Dickson DW (2011) Corticobasal degeneration: a pathologically distinct 4R tauopathy. Nat Rev Neurol 7:263–272

Kreczmanski P et al (2007) Volume, neuron density and total neuron number in five subcortical regions in schizophrenia. Brain 130:678–692

Kubis N et al (2000) Preservation of midbrain catecholaminergic neurons in very old human subjects. Brain 123(Pt 2):366–373

Lynd-Balta E, Haber SN (1994) Primate striatonigral projections: a comparison of the sensorimotor-related striatum and the ventral striatum. J Comp Neurol 345:562–578

Lyness SA, Zarow C, Chui HC (2003) Neuron loss in key cholinergic and aminergic nuclei in Alzheimer disease: a meta-analysis. Neurobiol Aging 24:1–23

Ma SY, Röyttä M, Rinne JO, Collan Y, Rinne UK (1995) Single section and disector counts in evaluating neuronal loss from the *substantia nigra* in patients with Parkinson's disease. Neuropathol Appl Neurobiol 21:341–343

Ma SY, Röytt M, Collan Y, Rinne JO (1999) Unbiased morphometrical measurements show loss of pigmented nigral neurones with ageing. Neuropathol Appl Neurobiol 25:394–399

McRitchie DA, Halliday GM, Cartwright H (1995) Quantitative analysis of the variability of *substantia nigra* pigmented cell clusters in the human. Neuroscience 68:539–551

Morris JC (1993) The clinical dementia rating (CDR): current version and scoring rules. Neurology 43:2412–2414

Mouton PR (2011) Unbiased stereology: a concise guide. The John Hopkins University Press, Baltimore

Muthane U, Yasha TC, Shankar SK (1998) Low numbers and no loss of melanized nigral neurons with increasing age in normal human brains from India. Ann Neurol 43(3):283–287

Ogisu K et al (2013) 3D neuromelanin-sensitive magnetic resonance imaging with semi-automated volume measurement of the *substantia nigra* pars compacta for diagnosis of Parkinson's disease. Neuroradiology 55:719–724

Pakkenberg B, Møller A, Gundersen HJ, AM Dam, Pakkenberg H (1991) The absolute number of nerve cells in substantia nigra in normal subjects and in patients with Parkinson's disease estimated with an unbiased stereological method. J Neurol Neurosurg Psychiatry 54:30–33

Perl DP, Good PF, Bussiere T, Morrison JH, Erwin JM, Hof PR (2000) Practical approaches to stereology in the setting of aging- and disease-related brain banks. J Chem Neuroanat 20:7–19

Pujol J, Junqué C, Vendrell P, Grau JM, Capdevila A (1992) Reduction of the *substantia nigra* width and motor decline in aging and Parkinson's disease. Arch Neurol 49:1119–1122

Rudow G, O'Brien R, Savonenko AV, Resnick SM, Zonderman AB, Pletnikova O, Marsh L, Dawson TM, Crain BJ, West MJ, Troncoso JC (2008) Morphometry of the human *substantia nigra* in ageing and Parkinson's disease. Acta Neuropathol 115(4):461–470

Schmithorst VJ, Dardzinski BJ, Holland SK (2001) Simultaneous correction of ghost and geometric distortion artifacts in EPI using a multiecho reference scan. IEEE Trans Med Imaging 20:535–539

Schmitz C (1998) Variation of fractionator estimates and its prediction. Anat Embryol 198:371–397

Schmitz C, Hof PR (2000) Recommendations for straightforward and rigorous methods of counting neurons based on a computer simulation approach. J Chem Neuroanat 20(1):93–114

Schmitz C, Korr H, Heinsen H (1999a) Design-based counting techniques: the real problems (letter). Trends Neurosci 22(8):345

Schmitz C, Rüb U, Korr H, Heinsen H (1999b) Nerve cell loss in the thalamic mediodorsal nucleus in Huntington's disease. II. Optimization of a stereological estimation procedure. Acta Neuropathol 97:623–628

Sohmiya M, Tanaka M, Aihara Y, Hirai S, Okamoto K (2001) Age-related structural changes in the human midbrain: an MR image study. Neurobiol Aging 22:595–601

Tanner C, Gilley D, Goetz C (1990) A brief screening questionnaire for parkinsonism. Ann Neurol 28:267–268

Theofilas P, Polichiso L, Wang X, Lima LC, Alho AT, Leite RE, Suemoto CK, Pasqualucci CA, Jacob Filho W, Heinsen H, Grinberg LT, Group BABS (2014) A novel approach for integrative studies on neurodegenerative diseases in human brains. J Neurosci Methods 226:171–183

UN (2013) World population prospects: the 2012 revision, vol Volume I: comprehensive tables ST/ESA/SER.A/336. United Nations

van Domburg PH, ten Donkelaar HJ (1991) The human *substantia nigra* and ventral tegmental area. A neuroanatomical study with notes on aging and aging diseases. Adv Anat Embryol Cell Biol 121:1–132

West MJ (1993) New stereological methods for counting neurons. Neurobiol Aging 14(4):275–285

West MJ, Ostergaard K, Andreassen OA, Finsen B (1996) Estimation of the number of somatostatin neurons in the striatum: an in situ hybridization study using the optical fractionator method. J Comp Neurol 370(1):11–22